REPORT

DYNAMIC GENOME

Dynamics of CTCF- and cohesin-mediated chromatin looping revealed by live-cell imaging

Michele Gabriele[1,2,3]†, Hugo B. Brandão[1,2,3]†‡, Simon Grosse-Holz[4,5]†, Asmita Jha[1,2,3], Gina M. Dailey[6], Claudia Cattoglio[6,7], Tsung-Han S. Hsieh[6,7], Leonid Mirny[4,5,8]*, Christoph Zechner[9,10,11,12]*, Anders S. Hansen[1,2,3]*

Animal genomes are folded into loops and topologically associating domains (TADs) by CTCF and loop-extruding cohesins, but the live dynamics of loop formation and stability remain unknown. Here, we directly visualized chromatin looping at the *Fbn2* TAD in mouse embryonic stem cells using super-resolution live-cell imaging and quantified looping dynamics by Bayesian inference. Unexpectedly, the *Fbn2* loop was both rare and dynamic, with a looped fraction of approximately 3 to 6.5% and a median loop lifetime of approximately 10 to 30 minutes. Our results establish that the *Fbn2* TAD is highly dynamic, and about 92% of the time, cohesin-extruded loops exist within the TAD without bridging both CTCF boundaries. This suggests that single CTCF boundaries, rather than the fully CTCF-CTCF looped state, may be the primary regulators of functional interactions.

Mammalian genomes are folded into loops and domains known as topologically associating domains (TADs) by the proteins CTCF and cohesin (*1*). Mechanistically, cohesin is thought to load on DNA and bidirectionally extrude loops until it is blocked by CTCF such that CTCF establishes TAD boundaries (*2*–*6*). Functionally, CTCF- and cohesin-mediated looping and TADs play critical roles in multiple nuclear processes, including regulation of gene expression, somatic recombination, and DNA repair (*1*). For example, TADs are thought to regulate gene expression by increasing the frequency of enhancer-promoter interactions within a TAD and by decreasing enhancer-promoter interactions between TADs (*7*). However, to understand how TADs and loops are formed and maintained and how they function, it is necessary to understand the dynamics of CTCF- and cohesin-mediated loop formation and loop lifetime.

[1]Department of Biological Engineering, Massachusetts Institute of Technology, Cambridge, MA 02139, USA. [2]The Broad Institute of MIT and Harvard, Cambridge, MA 02139, USA. [3]Koch Institute for Integrative Cancer Research, Cambridge, MA 02139, USA. [4]Department of Physics, Massachusetts Institute of Technology, Cambridge, MA 02139, USA. [5]Institut Curie, 75005 Paris, France. [6]Department of Molecular and Cell Biology, University of California, Berkeley, Berkeley, CA 94720, USA. [7]Howard Hughes Medical Institute, University of California, Berkeley, Berkeley, CA 94720, USA. [8]Institute for Medical Engineering and Sciences, Massachusetts Institute of Technology, Cambridge, MA 02139, USA. [9]Max Planck Institute of Molecular Cell Biology and Genetics, 01307 Dresden, Germany. [10]Center for Systems Biology Dresden, 01307 Dresden, Germany. [11]Cluster of Excellence Physics of Life, TU Dresden, 01307 Dresden, Germany. [12]Faculty of Computer Science, TU Dresden, 01187 Dresden, Germany.
***Corresponding author. Email: leonid@mit.edu (L.M.); zechner@mpi-cbg.de (C.Z.); ashansen@mit.edu (A.S.H.)**
†These authors contributed equally to this work.
‡Present address: Illumina Inc., San Diego, CA 92122, USA.

Although recent advances in single-cell genomics and fixed-cell imaging have made it possible to generate static snapshots of three-dimensional (3D) genome structures in single cells (*8*–*13*), live-cell imaging is required to understand the dynamics of chromatin looping (*14*). Furthermore, previous studies have yielded conflicting results as to whether loops are well defined in single cells (*8*–*13*), perhaps because of the difficulty associated with distinguishing bona fide CTCF- and cohesin-mediated loops from mere proximity that emerges stochastically (*14*). Recent pioneering work has visualized enhancer-promoter interactions (*15*–*17*) and long-range V(D)J–chromatin interactions (*18*) in live cells. However, the dynamics of loop formation and the lifetime of CTCF- and cohesin-mediated loops have not yet been quantified in living cells.

To visualize the dynamics of CTCF- and cohesin-mediated looping, we chose as our model system the loop holding together the two CTCF-bound boundaries of the 505-kb *Fbn2* TAD in mouse embryonic stem cells (mESCs). This TAD is verified to be CTCF dependent (*19*) and relatively simple because it only contains a single gene, *Fbn2*, which is not expressed in mESCs (Fig. 1A). We used genome editing to homozygously label the left and right CTCF sites of the *Fbn2* TAD with TetO and Anchor3 arrays, which we then visualized by coexpressing the fluorescently tagged binding proteins TetR-3x-mScarlet and EGFP-OR3 (*20*) [clone C36 (Fig. 1, B to D)]. We developed a comprehensive image analysis framework, *ConnectTheDots*, to extract trajectories of 3D loop anchor positions from the acquired movies (fig. S1). By optimizing 3D super-resolution live-cell imaging conditions (*14*), we could track *Fbn2* looping dynamics at 20-s resolution for >2 hours (Fig. 1D and movies S1 to S4). After DNA replication in the S/G_2 phase, it is no longer possible to reliably distinguish intrachromosomal from sister-chromosomal interactions (*14*). We therefore filtered out replicated and low-quality dots using a convolutional neural network (fig. S2). Thus, we only considered G_1 and early S-phase cells.

To validate our system for tracking *Fbn2* loop dynamics, we performed a series of control experiments. First, we confirmed using Micro-C (*21*, *22*) that our locus-labeling approach did not measurably perturb the *Fbn2* loop (Fig. 1A). Second, to "mimic" the looped state, we deleted the 505 kb between the CTCF sites, generating clone C27 ("ΔTAD"; Fig. 1C). As expected, this reduced the 3D distance (Fig. 1E; the nonzero 3D distance distribution for C27 was expected because of localization noise and the 5-kb tether between CTCF sites and fluorescent labels; see fig. S3). Third, as a negative control for CTCF-mediated looping, we generated clone C65 ("ΔCTCFsites"; Fig. 1C) by homozygously deleting the three CTCF motifs in the *Fbn2* TAD (L1, L2, R1; Fig. 1A) and validated that this resulted in a loss of CTCF binding and cohesin colocalization using chromatin immunoprecipitation sequencing [ChIP-seq (fig. S4)]. As expected, the 3D distance increased in C65 (Fig. 1E). Next, we calculated mean-squared displacements (MSDs) of the relative positions of the two loci (two-point MSD), which are unaffected by cell movement. Chromatin dynamics were consistent with Rouse polymer dynamics, with a scaling of MSD ~ $t^{0.5}$ for all three clones (*23*) (Fig. 1F). We conclude that our approach faithfully reports on CTCF looping dynamics in live cells without noticeable artifacts.

To elucidate the specific roles of CTCF and cohesin, we endogenously tagged RAD21, CTCF, and the cohesin unloader WAPL with mAID in the C36 (WT) line, allowing for degradation with indole-3-acetic acid (*24*). For RAD21 and CTCF, we achieved near-complete depletion in 2 hours (fig. S5), long-term depletion led to cell death (fig. S6), Micro-C analysis revealed loss of the *Fbn2* loop or corner peak as expected (*25*–*28*) (Fig. 2A), and ChIP-Seq analysis showed a loss of chromatin binding (fig. S7). For WAPL, depletion took 4 hours and was less complete (fig. S5), long-term depletion occasionally yielded visibly compacted "vermicelli" chromosomes (*29*) (fig. S6C), and Micro-C analysis revealed increased corner peak strength (*27*, *28*, *30*) (Fig. 2A). All three AID lines exhibited lower protein abundance, likely because of leaky protein depletion (fig. S8).

Having validated the AID cell lines, we next performed live-cell imaging to study the specific roles of RAD21, CTCF, and WAPL in loop extrusion in vivo. Consistent with RAD21 being required for loop extrusion, RAD21 depletion

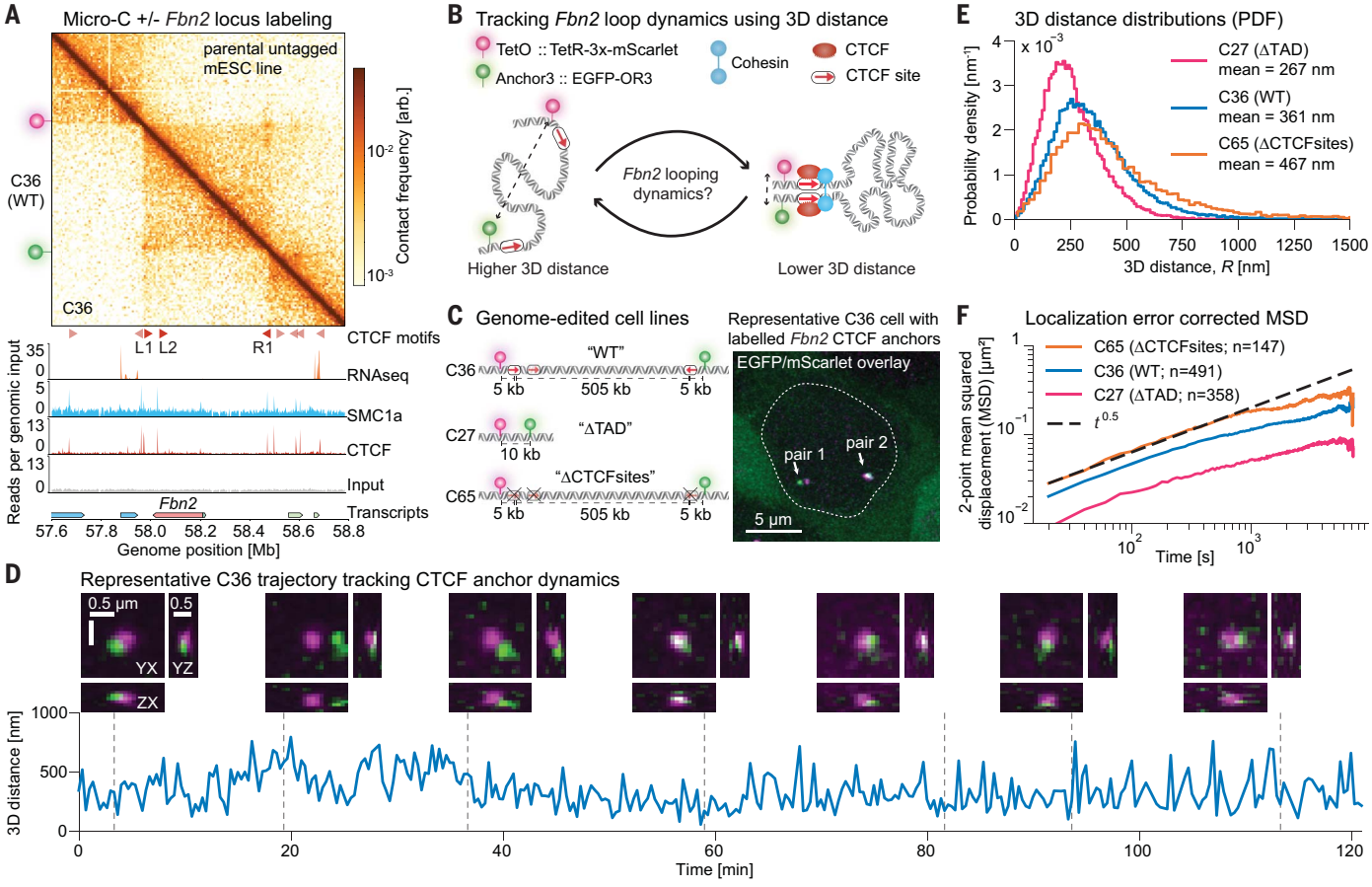

Fig. 1. Endogenous labeling and tracking of the *Fbn2* loop with super-resolution live-cell imaging. (**A**) Fluorescent labeling of *Fbn2* loop anchors does not perturb the *Fbn2* TAD. Shown is a Micro-C contact map comparing the parental untagged (C59, top left) and tagged (C36, bottom right) cell lines. Red triangles are CTCF motifs with orientation. C36 ChIP-seq shows CTCF (GSM3508478) and cohesin (SMC1A; GSM3508477) binding compared with input (GSM3508475). *Fbn2* is not expressed (RNA-seq GSE123636; annotation: GRCm38). Genome coordinates: mm10. (**B**) Overview of tagging and readout using 3D distance. (**C**) Overview of the genome-edited cell lines (left) and a representative maximum intensity projection (MIP) of a cell nucleus showing two pairs of "dots" (right). (**D**) Representative 3D trajectory over time of a dot pair. MIPs of the 3D voxels centered on the mScarlet dot (top) and 3D distances between dots (bottom) are shown. (**E**) 3D distance probability density functions of dot pairs (n = 32,171, n = 46,163, and n = 13,566 distance measurements for C27, C36, and C65, respectively). (**F**) Localization error–corrected two-point MSD plots (n = 358, n = 491, and n = 147 trajectories in C27, C36, and C65, respectively).

strongly increased the 3D distances (Fig. 2, B and C). Consistent with CTCF being the boundary factor that is required for *Fbn2* loop formation (Fig. 1B) but not required for loop extrusion, CTCF depletion increased 3D distances, albeit less than RAD21 depletion (*6*). Finally, consistent with prior observations that WAPL depletion increases cohesin residence time and abundance on chromatin (*29*), potentially allowing it to extrude longer and more stable loops (*27*, *30*), WAPL depletion decreased the 3D distances (Fig. 2, B and C).

To quantify the extent of loop extrusion of the *Fbn2* TAD, we turned to polymer physics theory. The Rouse model predicts a linear relationship between chain length and mean squared distance ($<R^2>$) between the fluorescent labels (dashed lines in Fig. 2D; see also fig. S9). By assuming that ΔRAD21 represents the fully unextruded state with a genomic separation of 515 kb (Fig. 1C), we could then assign an "effective tether length" (i.e., the unextruded fraction) to each condition. We found an effective tether length of ~200 kb in C36 (WT) and ~280 kb in ΔCTCF, corresponding to ~39 and ~54% of the full genomic separation, respectively. By subtraction, the genomic separation between the two labels shortened by ~46% due to extrusion alone (ΔRAD21 versus ΔCTCF) and by ~61% due to extrusion with boundaries (ΔRAD21 versus C36). This shows that by blocking extruding cohesins, CTCF increases the fraction extruded between the two CTCF boundaries. Overall, we estimate that, on average, just over half of the *Fbn2* TAD is extruded.

By combining these measurements (Fig. 2, B to D) with our Micro-C data (Fig. 2A), we were then able to determine dynamic parameters of our polymer model of loop extrusion (Fig. 2, E and F), including spacing between cohesins and their processivity, as well as the total strength of the CTCF boundaries (see the supplementary materials). Consistent with our ΔRAD21 data, our polymer simulations resulted in chromosome decompaction after near-complete RAD21 depletion (Fig. 2E) and accurately matched our experimental data (Fig. 2F).

Next, we sought to identify where and when CTCF-CTCF loops occured in our trajectories. Because of localization noise and substantial temporal correlations in the data, simple analysis methods failed when benchmarked on simulations (see the supplementary text). Therefore, we developed Bayesian inference of looping dynamics (BILD). In BILD, we coarse-grained the possible conformations of the TAD (Fig. 3A) into two states: (i) a state of sustained contact between the CTCF sites, presumably mediated by cohesin (the "looped state"), and (ii) all other possible conformations, including partial extrusion, random contacts, and the fully unlooped conformation (the "unlooped state"). While the looped state relies on CTCF activity, the unlooped

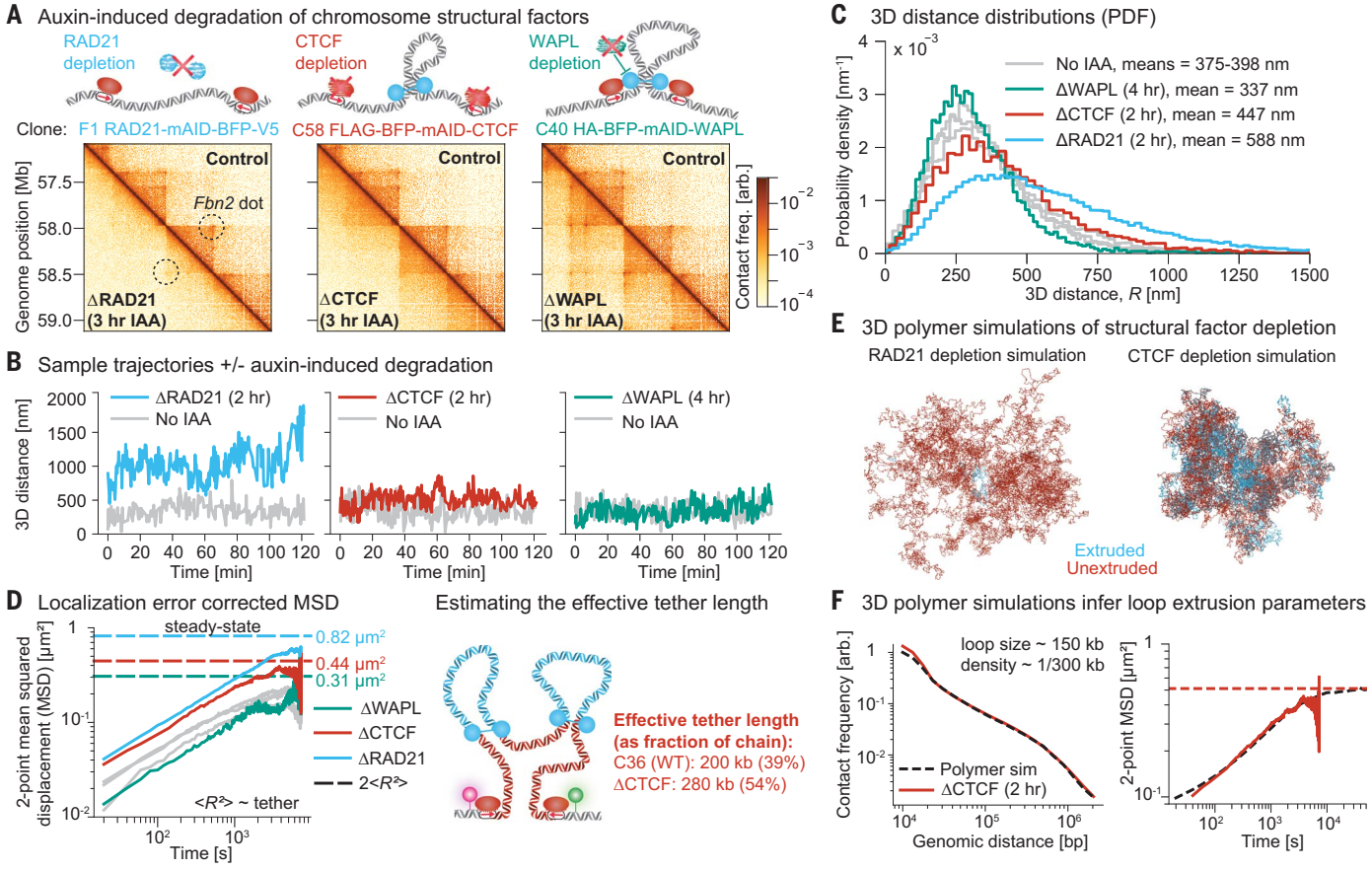

Fig. 2. Degradation of CTCF, cohesin, and WAPL reveals their role in loop extrusion and looping-mediated chromosome compaction. (**A**) Micro-C data for the AID-tagged clones for RAD21 (left), CTCF (middle), and WAPL (right) showing control data [no indole-3-acetic acid (IAA) treatment; top half] and protein degradation data (3 hours after IAA; bottom half), with schematics illustrating the expected effect. (**B**) Representative trajectories with (colored lines) or without (gray lines) IAA treatment for each AID-tagged clone. (**C**) 3D distance probability density functions of dot pairs [n = 45,379, n = 10,469, and n = 18,153 distance measurements for ΔRAD21 (2 hours), ΔCTCF (2 hours), and ΔWAPL (4 hours) depletion conditions, respectively, and n = 17,605, n = 11,631, and n = 21,001 for the same clones without treatment]. (**D**) Localization error–corrected two-point MSD plots for the AID-tagged clones (left) [n = 537, n = 137, and n = 215 trajectories in ΔRAD21 (2 hours), ΔCTCF (2 hours), and ΔWAPL (4 hours) depletion conditions, respectively, and n = 183, n = 151, and n = 257 for the same clones without treatment (gray lines)]. The effective tether length was obtained by computing the ratio of the steady-state variance of each clone to the value in the RAD21-depletion condition (note that $2\langle R^2\rangle$ is also the asymptotic value of the MSD; see also the supplementary materials). (**E**) Representative 3D polymer conformation from simulations mimicking the ΔRAD21 (95% cohesin depletion) (left) and ΔCTCF (100% CTCF depletion) (right) depletion conditions. Red is the unextruded segment, blue the extruded segment. (**F**) Matching simulations to the data to obtain loop-extrusion parameters (three fit parameters; see the supplementary materials).

state reflects extrusion without bridged CTCF boundaries, resembling the ΔCTCF condition. On the basis of the MSD~$t^{0.5}$ scaling observed in Fig. 2D, we modeled the unlooped state as a free Rouse chain calibrated to the ΔCTCF data (fig. S10). To model the looped state, we introduced an additional bond between the two CTCF sites (Fig. 3B); this bond is switchable, allowing transitions between the looped and unlooped states. The length of the bond was set to reproduce the 10-kb distance between the fluorophores, using ΔRAD21 as reference for a free 515-kb chain (see the supplementary text). Finally, by using a hierarchical Bayesian model (*31*), BILD then exploited the different spatiotemporal dynamics of the looped state to infer which segments of each trajectory were in the looped state (purple segment in Fig. 3A). When tested on 3D polymer simulations with experimentally realistic noise, BILD accurately inferred both the looped fraction and the loop lifetime (Fig. 2, E and F, and figs. S11 and S12). In summary, BILD allows us to distinguish CTCF- and cohesin-mediated looping from mere proximity.

We next used BILD to infer looping in our experimental trajectory data (Fig. 3, C to F). BILD revealed that the *Fbn2* TAD was fully looped ~6.5% (~3%) of the time, but spent ~93.5% (97%) of the time in a fully unlooped or partially extruded conformation (Fig. 3E). We use brackets to indicate the looped fraction after false-positive correction (fig. S12; the corrected looped fraction was ~6% when we calibrated BILD using a 15-kb fluorophore distance; fig. S13). By contrast, we observed a minimal looped fraction of ~2% (~0%) in ΔRAD21 and ΔCTCF and ~4% (~1%) in C65 (ΔCTCFsites), whereas the looped fraction was increased to ~10% (~6%) in ΔWAPL, consistent with WAPL unloading cohesin from chromatin (*29*).

Finally, we estimated the lifetime of the looped state (Fig. 3, D and F). Accurate measurement of loop lifetimes from finite trajectories can be challenging when trajectories begin or end in the looped state, so that it is unclear how long the looped period truly lasted (e.g., the looped state in the ΔWAPL trajectory in Fig. 3D existed an unknown time before the

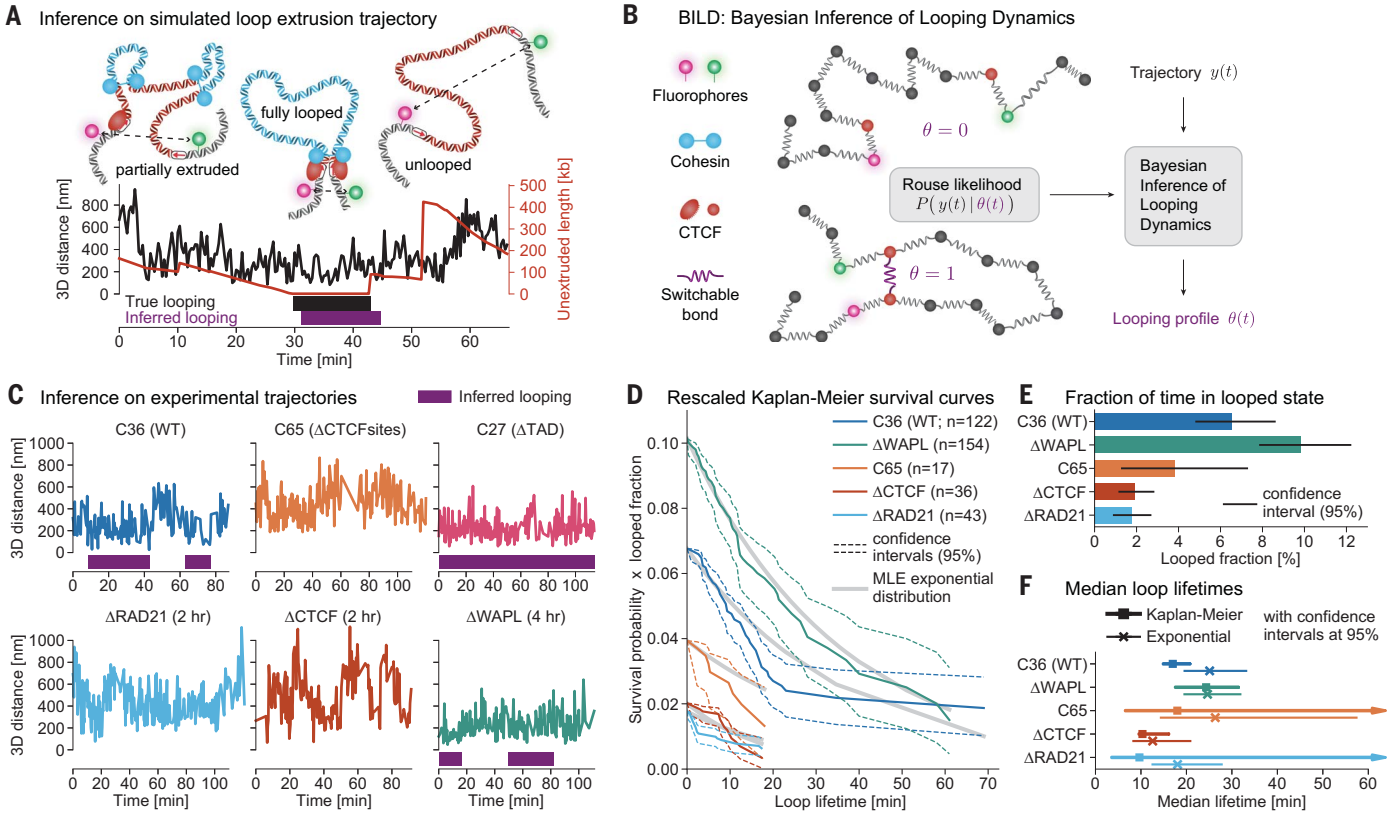

Fig. 3. BILD reveals rare and dynamic CTCF loops. (**A**) Example trajectory from polymer simulations with loop extrusion. Extrusion shortens the effective tether (red is the unextruded length, ground truth from simulations) between the CTCF sites. A ground truth loop is formed when the tether is minimal and cohesin is stalled at both CTCF sites (black bar). BILD captures these accurately (purple bar). (**B**) Schematic overview of BILD. Building on the analytical solution to the Rouse model, we used a hierarchical Bayesian model to determine the optimal looping profile for single trajectories. (**C**) Illustrative examples of inferred looping on real trajectory data. (**D**) Kaplan-Meier survival curves rescaled by the inferred looped fraction. Gray lines are maximum likelihood fits of a single exponential to the data, accounting for censoring. (**E**) Fraction of time the *Fbn2* locus spends in the fully looped conformation. Error bars are bootstrapped 95% confidence intervals. (**F**) Median loop lifetimes from the Kaplan-Meier survival curves (squares) or exponential fits (crosses). Confidence intervals are determined from the confidence intervals on the Kaplan-Meier curve and the likelihood function of the exponential fit, respectively. Where the upper confidence limit on the survival curve did not cross below 50%, an arrowhead indicates a semi-infinite confidence interval.

start of the movie). This problem, known in medical statistics as "censoring," can be solved using the Kaplan-Meier survival estimator. Using this approach, we obtained censoring-corrected survival curves (Fig. 3D) of the looped state, from which we estimated the median loop lifetime (Fig. 3F). Orthogonal to this non-parametric analysis, we also fitted an exponential model, yielding similar estimates. Together, these results give an estimate of the median loop lifetime of ~10 to 30 min in C36 (WT) (Fig. 3F and fig. S12D). These results revealed the fully looped state to be both rare (~3 to 6%) and dynamic (median ~10 to 30 min; mean ~15 to 45 min). Thus, during an average ~12-hour mESC cell cycle, the looped state will occur approximately one or two times, lasting cumulatively ~20 to 45 min, but the remaining ~11.5 hours will be in the partially extruded or fully unlooped conformations.

To understand whether a low looped fraction of ~3% is consistent with a clear and strong corner peak in the Micro-C map, we set up polymer simulations with loop extrusion. Consistent with recent reports, we found that CTCF-mediated stabilization of cohesin was necessary to reproduce both of these features in our simulations (Fig. 4 and fig. S14). We confirmed this effect using inverse fluorescence recovery after photobleaching (iFRAP) of cohesin, finding that CTCF depletion decreased cohesin residence time (fig. S15). Incorporating this effect, we then simulated loop extrusion with a cohesin density of 1/240 kb and processivity of 150 kb (processivity = lifetime × extrusion speed). When cohesin reaches a CTCF site, it has a 12.5% probability of stalling, which, using the estimate of 50% CTCF occupancy (*34*), translates into an ~25% capture efficiency of CTCF. Once stalled on one side by CTCF, cohesin is stabilized fourfold beyond its base lifetime of ~20 min (*35*) (fig. S14), facilitating the formation of longer loops because the other side of cohesin may continue to extrude. These simulations reproduced both our experimental Micro-C maps (Fig. 4A) and the median loop lifetime and low looped fraction (Fig. 4B).

Together, these results allow us to paint a comprehensive mechanistic picture of the *Fbn2* TAD (Fig. 4, C and D). Most of the time (~92%), the TAD is partially extruded, with ~57 to 61% of the *Fbn2* region captured in one to three extruding cohesin loops, whereas ~39 to 43% remain unextruded. The fully unlooped conformation, as would be found in the absence of cohesin, occurs only ~6% of the time, whereas the fully looped state is even more rare at ~3% (~2% in simulations) and has a median lifetime of ~10 to 30 min. Our simulations reveal that the looped state is sometimes held together by multiple cohesins (Fig. 4C), which also explains why the loop lifetime can be substantially shorter than the CTCF-stabilized cohesin lifetime. We stress

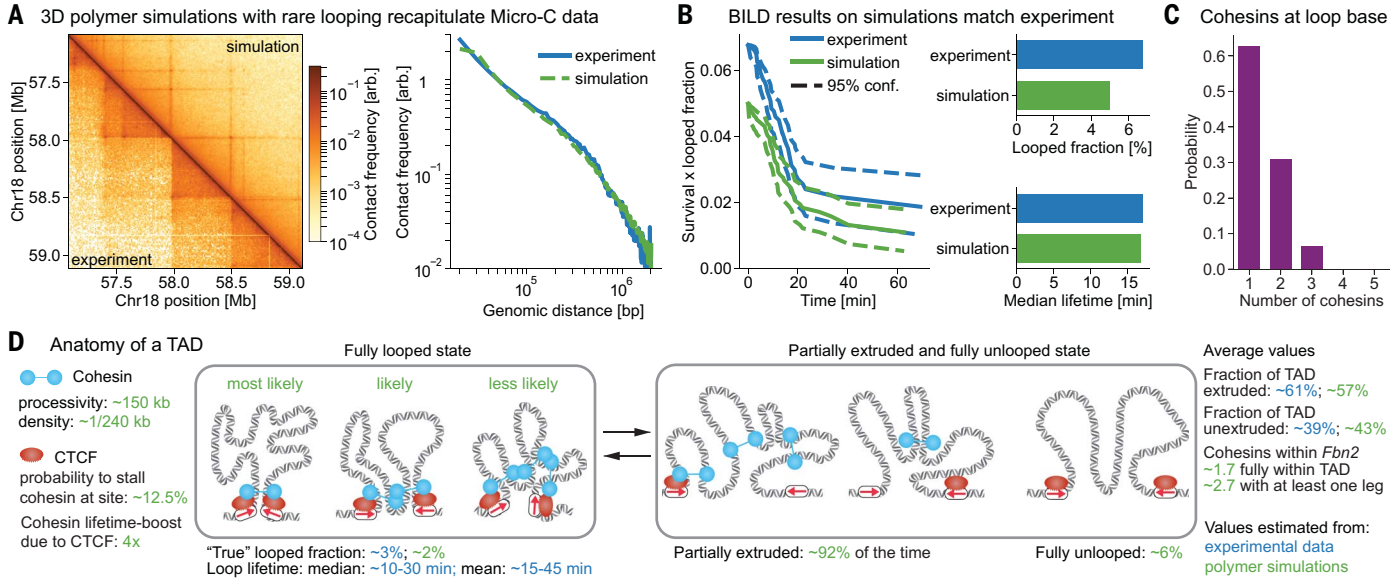

Fig. 4. Comprehensive picture of the *Fbn2* TAD. (**A**) Comparison of Micro-C data for the C36 (WT) line with in silico Micro-C of our best-fit simulation map (left) and contact probability scaling (right). (**B**) BILD applied to the same simulation (green) compared with C36 (WT) experimental data (blue). (**C**) Number of cohesins forming the looped state in simulations (n = 18,789). (**D**) "Anatomy" of the *Fbn2* TAD. Quantitative description of the *Fbn2* TAD is shown using both real data (blue) and our best-fit simulation (green). Cohesin processivity and density and CTCF stalling probability and lifetime boost are simulation parameters. Fraction of time in different conformations was extracted from simulation ground truth using effective tether lengths of 1.1 and 505 kb as cutoffs to define "fully looped" and "fully unlooped," respectively. The fraction of TAD that was unextruded was calculated using the mean tether length over the full simulation.

that both the mechanistic assumptions of our polymer models and the experimental data constraining them are associated with uncertainty, resulting in uncertainty of the inferred parameters (Fig. 4D). For example, if we allow extruding cohesins to bypass each other in our simulations (*36*, *37*), then our estimates of the fold stabilization of cohesin by CTCF would change from approximately fourfold to approximately twofold, the CTCF stalling probability would change from 12.5 to 25%, and the looped state would now be held together by a single cohesin (fig. S16). We also note that TADs smaller than the 505-kb *Fbn2* TAD and TADs with stronger CTCF boundaries may have a higher looped fraction (*38*). Accordingly, we propose that our absolute quantification of the *Fbn2* looped fraction may now allow calibrated inference of absolute looped fractions genome wide on the basis of Micro-C (*13*).

Our findings reveal that the CTCF- and cohesin-mediated looped state that holds together CTCF boundaries of TADs is rare, dynamic, and transient. A key limitation of our study is that it represents just one loop in one cell type. Nevertheless, the *Fbn2* loop is among the strongest quartile of "corner peaks" in Micro-C maps, suggesting that most other similarly sized loops in mESCs are likely weaker than *Fbn2* (fig. S17). Our results thus rule out static models of TADs that exist in either a fully unlooped state or a fully looped state stably bridged by one cohesin (Fig. 1B). Instead, we show that the *Fbn2* TAD most often exists in a partially extruded state formed by a few cohesins in live cells (~92%; Fig. 4D), and that when the rare looped state is formed, it is transient (~10 to 30 min median lifetime; Fig. 4B). Because the partially extruded state dominates, this may be the functionally important TAD state. Thus, we suggest that CTCF-mediated transcriptional insulation may be mediated more by individual extrusion-blocking CTCF boundaries than by the rare fully looped state. Similarly, this suggests that regulatory interactions, such as those between enhancers and promoters, may depend more on frequent cohesin-mediated contacts within a TAD rather than rare CTCF-CTCF loops. This dynamic picture of TADs in live cells (Fig. 4D) may also help to explain cell-to-cell variation in 3D genome structure, and consequently stochasticity in downstream processes such as gene expression and cell differentiation.

REFERENCES AND NOTES

1. J. A. Beagan, J. E. Phillips-Cremins, *Nat. Genet.* **52**, 8–16 (2020).
2. M. Ganji *et al.*, *Science* **360**, 102–105 (2018).
3. Y. Kim, Z. Shi, H. Zhang, I. J. Finkelstein, H. Yu, *Science* **366**, 1345–1349 (2019).
4. I. F. Davidson *et al.*, *Science* **366**, 1338–1345 (2019).
5. S. Golfier, T. Quail, H. Kimura, J. Brugués, *eLife* **9**, e53885 (2020).
6. G. Fudenberg *et al.*, *Cell Rep.* **15**, 2038–2049 (2016).
7. O. Symmons *et al.*, *Genome Res.* **24**, 390–400 (2014).
8. M. V. Arrastia *et al.*, *Nat. Biotechnol.* **40**, 64–73 (2022).
9. Q. Szabo *et al.*, *Sci. Adv.* **4**, eaar8082 (2018).
10. T. J. Stevens *et al.*, *Nature* **544**, 59–64 (2017).
11. E. H. Finn *et al.*, *Cell* **176**, 1502–1515.e10 (2019).
12. B. Bintu *et al.*, *Science* **362**, eaau1783 (2018).
13. D. I. Cattoni *et al.*, *Nat. Commun.* **8**, 1753 (2017).
14. H. B. Brandão, M. Gabriele, A. S. Hansen, *Curr. Opin. Cell Biol.* **70**, 18–26 (2021).
15. H. Chen *et al.*, *Nat. Genet.* **50**, 1296–1303 (2018).
16. J. M. Alexander *et al.*, *eLife* **8**, e41769 (2019).
17. Z. Hensel, X. Weng, A. C. Lagda, J. Xiao, *PLOS Biol.* **11**, e1001591 (2013).
18. N. Khanna, Y. Zhang, J. S. Lucas, O. K. Dudko, C. Murre, *Nat. Commun.* **10**, 2771 (2019).
19. E. de Wit *et al.*, *Mol. Cell* **60**, 676–684 (2015).
20. T. Germier *et al.*, *Biophys. J.* **113**, 1383–1394 (2017).
21. T. S. Hsieh *et al.*, *Mol. Cell* **78**, 539–553.e8 (2020).
22. A. S. Hansen *et al.*, *Mol. Cell* **76**, 395–411.e13 (2019).
23. H. Hajjoul *et al.*, *Genome Res.* **23**, 1829–1838 (2013).
24. T. Natsume, T. Kiyomitsu, Y. Saga, M. T. Kanemaki, *Cell Rep.* **15**, 210–218 (2016).
25. S. S. P. Rao *et al.*, *Cell* **171**, 305–320.e24 (2017).
26. E. P. Nora *et al.*, *Cell* **169**, 930–944.e22 (2017).
27. G. Wutz *et al.*, *EMBO J.* **36**, 3573–3599 (2017).
28. T.-H. S. Hsieh *et al.*, Enhancer-promoter interactions and transcription are maintained upon acute loss of CTCF, cohesin, WAPL, and YY1. bioRxiv 2021.07.14.452365 [Preprint] (2021); https://www.biorxiv.org/content/10.1101/2021.07.14.452365v1.
29. A. Tedeschi *et al.*, *Nature* **501**, 564–568 (2013).
30. J. H. I. Haarhuis *et al.*, *Cell* **169**, 693–707.e14 (2017).
31. C. M. Bishop, *Pattern Recognition and Machine Learning (Information Science and Statistics)* (Springer-Verlag, 2006).
32. Y. Li *et al.*, *Nature* **578**, 472–476 (2020).
33. G. Wutz *et al.*, *eLife* **9**, e52091 (2020).
34. C. Cattoglio *et al.*, *eLife* **8**, e40164 (2019).
35. A. S. Hansen, I. Pustova, C. Cattoglio, R. Tjian, X. Darzacq, *eLife* **6**, e25776 (2017).
36. E. Kim, J. Kerssemakers, I. A. Shaltiel, C. H. Haering, C. Dekker, *Nature* **579**, 438–442 (2020).
37. H. B. Brandão, Z. Ren, X. Karaboja, L. A. Mirny, X. Wang, *Nat. Struct. Mol. Biol.* **28**, 642–651 (2021).
38. P. Mach *et al.*, Live-cell imaging and physical modeling reveal control of chromosome folding dynamics by cohesin and CTCF. bioRxiv 2022.03.03.482826 [Preprint] (2022);

https://www.biorxiv.org/content/10.1101/2022.03.03.482826v1.
39. H. B. Brandão, ConnectTheDots: A chromosome locus pair tracking library, Zenodo (2022); https://zenodo.org/record/6224612.
40. S. Grosse-Holz, SGrosse-Holz/tracklib: initial release, Zenodo (2022); https://zenodo.org/record/6144781.
41. M. Gabriele *et al*., Trajectory data for: Dynamics of CTCF and cohesin mediated chromatin looping revealed by live-cell imaging, Zenodo (2021); https://doi.org/10.5281/zenodo.5770531.

ACKNOWLEDGMENTS

We thank R. Tjian and X. Darzacq for hosting early parts of this work; J. Alexander for providing the RNA destabilization elements; L. Joh for assistance with cloning; and members of the Hansen, Zechner, and Mirny laboratories for insightful discussions. **Funding:** This work was supported by the National Institutes of Health (grants R00GM130896, DP2GM140938, and R33CA257878 to A.S.H.; grant UM1HG011536 to A.S.H. and L.M.; and grant R01GM114190 to L.M.); the National Science Federation (grant 2036037 to A.S.H.); the Mathers' Foundation (A.S.H.); a Pew-Stewart Cancer Research Scholar grant (A.S.H.); Chaires d'excellence internationale Blaise Pascal (L.M.); an American-Italian Cancer Foundation research fellowship (M.G.); and core funding from the Max Planck Institute of Molecular Cell Biology and Genetics (C.Z.). **Author contributions:** A.S.H. conceived and initiated the project. H.B.B., M.G., S.G.H., L.M., C.Z., and A.S.H. designed the project. A.S.H. performed genome editing and generated the cell lines. G.M.D. cloned plasmids. M.G., A.J., C.C., and A.S.H. characterized and validated the cell lines. T.H.S.H. performed Micro-C. C.C. performed ChIP-Seq. M.G., A.J., and H.B.B. optimized imaging experiments with input from A.S.H. M.G., A.J., and H.B.B. collected the imaging data, with acquisition led by M.G. and A.J.; M.G. and A.J. performed control experiments and characterized the AID cell lines. H.B.B. developed the image-processing pipeline and analyzed the imaging data, with input from A.S.H., S.G.H., M.G., and A.J.; H.B.B. and S.G.H. developed the convolutional neural network, with input from A.S.H., M.G., and A.J.; H.B.B. performed polymer simulations with input from S.G.H. and L.M. M.G., A.J., H.B.B., and A.S.H. annotated trajectory data. S.G.H. and C.Z. designed BILD with input from H.B.B., L.M., and A.S.H. S.G.H. developed and benchmarked BILD, applied BILD to trajectory data, and developed MSD analysis with input from H.B.B., L.M., A.S.H., and C.Z. H.B.B. and S.G.H. analyzed polymer simulations. A.S.H., L.M., and C.Z. supervised the project. H.B.B., M.G., S.G.H., A.J., and A.S.H. drafted the manuscript and figures. All authors edited the manuscript and figures. **Competing interests:** The authors declare no competing interests. **Data and materials availability:** Cell lines, plasmids, and other materials are available upon request. All cell lines used in this study use the ANCHOR3 system for DNA locus visualization licensed from NeoVirTech. Recipients of the cell lines will need to execute a materials transfer agreement with NeoVirTech. The code and software used in this study, including the image-processing framework *ConnectTheDots* (*39*) and *BILD* (part of tracklib) (*40*), are freely available as described in table S5. The Micro-C and ChIP-Seq data associated with this study are available at the Gene Expression Omnibus (https://www.ncbi.nlm.nih.gov/geo/) under accession number GSE187487. The raw trajectory data are available through Zenodo (*41*). For a list of all datasets used in this study, please see table S6.

SUPPLEMENTARY MATERIALS

science.org/doi/10.1126/science.abn6583
Materials and Methods
Supplementary Text
Figs. S1 to S17
Tables S1 to S6
References (*42*–*90*)
Movies S1 to S4
MDAR Reproducibility Checklist

View/request a protocol for this paper from *Bio-protocol*.

12 December 2021; accepted 31 March 2022
10.1126/science.abn6583

Science

Dynamics of CTCF- and cohesin-mediated chromatin looping revealed by live-cell imaging

Michele GabrieleHugo B. BrandãoSimon Grosse-HolzAsmita JhaGina M. DaileyClaudia CattoglioTsung-Han S. HsiehLeonid MirnyChristoph ZechnerAnders S. Hansen

Science, 376 (6592), • DOI: 10.1126/science.abn6583

Fleeting chromatin loops

The genome is organized into three-dimensional (3D) domains that are widely thought to be stable, fully looped structures, although this organization has not been directly observed in living cells. Gabriele *et al*. report the direct visualization of chromatin looping in living cells and use Bayesian inference to quantify looping dynamics. Loops were found to be both rare and short-lived, overturning static models of looping. Instead of being fully looped, 3D genome domains existed overwhelmingly in partially folded configurations. This more dynamic view of 3D genome domains may ultimately allow a deeper understanding of why disruption of some domains and loops causes dysregulation of gene expression in disease. —DJ